Trends in Chemical Engineering
Vol. 22, 2024

Original Article

Developing new nanocatalysts from calcium waste materials for biodiesel production

Samuel Santos[1], Jaime Puna[1,2] and João Gomes[1,2,*]

[1]CERENA—Center for Natural Resources and Instituto Superior Técnico, University of Lisbon, Av. Rovisco Pais, 1, 1049-001 Lisboa, Portugal; [2]Chemical Engineering Department, Instituto Superior de Engenharia de Lisboa, Lisbon Polytechnic, R. Conselheiro Emídio Navarro, 1, 1959-007 Lisboa, Portugal.

ABSTRACT

In this research work a heterogeneous (solid base) nanocatalyst, originating from calcium waste materials, was produced. Firstly, calcium oxide (CaO) obtained by calcination (850 ºC for three hours) of chicken eggshells was used as a benchmark catalyst in the transesterification reaction of soybean oil. This catalyst was characterised using several techniques: Scanning Electron Spectroscopy (SEM), Infra-Red Spectroscopy (FTIR), and Particle Size Distribution (PSD), that are adequate for determining the specific surface area and volume of micro- and mesopores. The structure of the obtained CaO consisted of several agglomerates of white granular solids, with particles ranging from 50 to 332 nm (average of 117 nm) in size and having a specific surface area of 15.3 m^2/g. Three different catalyst loadings were tested with regard to catalytic activity of calcium oxide under the same reaction conditions. Then, a nanocatalyst precursor, calcium acetate, was produced from the same eggshells used before. This precursor was then applied in a supercritical antisolvent (SAS) precipitation apparatus to control its particle size. After the precipitation, the precursor was calcined to convert it into nano-structured calcium oxide. This Nano-CaO was also characterised by the techniques used for the earlier referred benchmark catalyst and by Energy Dispersive X-ray spectroscopy (EDS) to identify the chemical elements present. The observed structure of this solid very much resembles the benchmark catalyst. However, the particle sizes are smaller, ranging from 23 to 453 nm (average of 77 nm) and have a specific area of 315.7 m^2/g, which meant that an increase in specific surface area was achieved by decreasing the particle size. Regarding catalyst activity, a small amount of Nano-CaO was tested at the same conditions as before, and the best results showed an increase of 9% in transesterification reaction yield.

KEYWORDS: biofuels, calcium oxide, nano-structured catalysts, solid base heterogeneous catalyst, transesterification.

1. Introduction

Research on new renewable energy sources as alternatives to fossil fuels has been increasing in the last decades due to the non-renewable nature of these resources, the rapid rise of fossil fuel prices, and the growing concerns about environment and health impacts [1-4]. The European Union (EU) aimed to replace around 10% of all transportation fuel consumed within the EU from fossil fuels with biofuels by the year 2020 [5, 6].

Biodiesel is a preferred replacement for petrodiesel in-vehicle internal combustion engines, bringing benefits such as renewability, availability, non-toxicity, greenhouse gas emission reduction, improvement of lubrification properties of the diesel fuel blend and superior cetane number, which could be easily adopted also in developing countries [7-9].

*Corresponding author: jgomes@deq.isel.ipl.pt

Compared to fossil fuels, the combustion of biodiesel results in more than 90% decrease in total unburned hydrocarbons and a decrease in polycyclic aromatic hydrocarbon emissions ranging from 75 to 90% [10, 11]. Biodiesel can be mixed with petrodiesel at any weight ratio or percentage, and it can be used without blending with fossil fuels (B100), making it a successful fuel [12].

Its production from biological sources such as vegetable oils, microalgae, animal fats and waste cooking oils has been thoroughly reviewed [13-16]. The most common industrial process to produce biodiesel from vegetable oils or fats, involves alkaline homogeneous catalysts.

Nevertheless, the transesterification of triglycerides using basic homogeneous catalysts presents some drawbacks like its susceptibility to the oil purity, since an excess of free fatty acids (FFA) will promote the formation of water and soap due to the reaction between the FFA and the basic catalyst. This saponification reaction is undesired as the formed soap will contribute to lowering the transesterification yield and hinder the separation of the esters from glycerol. Another drawback is the large amounts of contaminated effluents generated during the pH neutralisation and Fatty Acid Methyl-Ester (FAME) purification stages in the industrial process [17–25].

A good alternative would be the use of solid-base catalysts. A great variety of basic materials such as (i) single alkaline earth metal oxides (MgO, BeO, CaO, SrO, BaO and RaO) and other single metal oxides (SnO_2, ZnO and CeO_2); (ii) supported alkali metal and alkaline earth metal oxides ($CaZrO_3$, Al_2O_3-SnO, Li/MgO, Al_2O_3/KI, KOH/Al_2O_3, KOH/NaY (KOH/ sodium crystal structure Y) and supported alumina/silica supported K_2CO_3); (iii) mixed metal oxides; (iv) hydrotalcites; and (v) anionic ion-exchange resins have been utilised as heterogeneous catalysts to perform the alcoholysis process [26-36]. Out of these catalysts, alkaline earth metal oxides have been widely employed as solid-base catalysts because of their high basic strength and relatively low cost. CaO waste materials have a good potential to be used as solid-base catalysts in the transesterification of triglycerides to produce biodiesel since they exhibit high basicity when compared to alkaline homogeneous catalysts, amongst other advantages like being cheap, non-corrosive and economically benign as they originate from natural sources such as seafood shells and waste eggs (~95% $CaCO_3$) [37-44]. It should be noted that the rate of the transesterification process using heterogeneous catalysts is typically lower than the process using homogeneous alkali catalysts which is due to a slow diffusion of reactants towards the active sites. This phenomenon occurs in solid catalysts, which are associated with the existence of a more complex three-phase system such as this system, consisting of oil-methanol-solid catalyst [45, 46].

A good approach to solve this problem could be the use of nanocatalysts. Nanocatalysts have higher specific surface area and, thus, catalytic activities, which may solve the above-mentioned problems [47]. Some of the most used methods for the production of nanomaterials are gas condensation, vacuum deposition and evaporation, impregnation, chemical vapor deposition, precipitation, calcination-hydration-dehydration, nano-grinding, sol-gel techniques, and so forth [4, 48-50]. Supercritical antisolvent precipitation (SAS) has been proposed as an innovative, environmentally friendly technology to prepare nanomaterials far more efficiently than liquid solvent precipitation. Supercritical CO_2 ($scCO_2$) as an antisolvent that provides the controlled precipitation of solids dissolved in conventional solvents has been applied in the production of a range of materials, including polymers, biopolymers, superconductors, explosives, dyes, active pharmaceutical ingredients (APIs) and catalysts if the processed compounds are insoluble in the supercritical medium [51-57].

In this work, the CaO used was obtained from natural sources, (in this particular case, chicken eggshells), as a nanocatalyst, by applying the SAS technique for the catalyst micronization. This technique uses a solution of CaO in conventional liquid solvents. Then, the solvents are saturated by supercritical CO_2, resulting in the controlled precipitation of nanocrystalline CaO through the anti-solvent effect [58, 59]. The nanocatalysts thus obtained were fully studied with regard to the transesterification reaction of soybean oil producing biodiesel.

2. Materials and Methods

2.1. Materials

The soybean oil was purchased from a local supermarket in Lisbon, Portugal. Methanol was of laboratory grade (MeOH, >99% pure), with CAS number 67-56-1. *Gallus gallus domesticus* (chicken) eggshells were collected from several households. Dimethyl sulfoxide (DMSO) was purchased from Merck with a purity of 99%, and glacial acetic acid was from Chem-Lab with CAS numbers 67-68-5 and 64-19-7.

2.2. Preparation of the catalyst

All the catalysts tested in this work were prepared from waste materials rich in calcium. Materials such as eggshells and seafood shells, except for shrimps, prawns, and barnacles (due to their high organic matter content), are highly available in nature, relatively cheaper and can produce calcium oxide (CaO) through their calcination.

It should be mentioned that among the heterogeneous catalysts used for transesterification reactions, calcium oxide (CaO) is widely used as it is cheap, non-corrosive, easy to handle and has high basicity compared to homogeneous base catalysts, e.g., NaOH and KOH. Nevertheless, the use of heterogeneous catalysts is a time-consuming process, as these catalysts need high reaction time to achieve high FAME yields and present some mass transfer limitations.

A solution to overcome these problems might be using CaO nanocatalysts, as they present higher surface area and catalytic activity, thereby significantly improving transesterification efficiency, resulting in faster reactions, i.e., shorter reaction times, low reaction temperatures and lower catalyst concentration. In this work, chicken eggshells were used as a precursor for the two types of catalysts: calcium oxide and calcium oxide nanocatalyst.

2.2.1. Calcium oxide (CaO) catalyst

In order to prepare this catalyst, eggshells were repeatedly washed in boiling water and dried in an oven set to 110 °C overnight. Afterwards, the dried eggshells were ground into a fine powder until the particle size achieved the desired diameter (< 500 μm). To finally convert the eggshells into calcium oxide, the calcination of the calcium carbonate took place, as described by Equation (1):

$$CaCO_3(s) \xrightarrow{850\ ^\circ C} CaO(s) + CO_2(g) \quad (1)$$

This calcination of calcium carbonate was performed in a muffle furnace (Heraeus K 114) at a temperature of 850 ºC for three hours.

After the calcination, the obtained calcium oxide was collected and stored inside a desiccator to ensure the complete absence of humidity, thus preventing the transformation of the calcium oxide into calcium hydroxide ($Ca(OH)_2$).

2.2.2. Calcium oxide (CaO) nanocatalyst precursor

A nanocatalyst precursor was prepared from the same batch of eggshells used for the CaO catalyst. The process started by converting the $CaCO_3$ present in the eggshells into calcium acetate [($Ca(CH_3COO)_2$) or $CaAc_2$] through the reaction with an aqueous acetic acid (CH_3COOH, 30 %wt). The calcium acetate precursor was later fed to the supercritical antisolvent (SAS) apparatus for the micronization process. The following reaction describes the precursor preparation process:

$$CaCO_3(s) + 2CH_3COOH\ (aq) \rightarrow Ca(CH_3COO)_2\ (aq) + H_2O\ (l) + CO_2\ (g) \quad (2)$$

The reaction was deemed as complete when all the $CaCO_3$ disappeared, and no more CO_2 was released.

Then, the remaining organic matter was filtered under vacuum. The filtrate was then processed by rotary evaporation, removing the solvent mixture. The obtained solid was collected in order to be used afterwards in the Supercritical Anti-solvent (SAS) process.

2.3. Supercritical anti-Solvent (SAS) apparatus

The calcium acetate obtained before was dissolved in a solution of Dimethyl sulfoxide (DMSO) and acetic acid (in equal volumetric parts) with a concentration of 20 mg/mL at room temperature to allow the micronization process to occur inside the SAS apparatus. The micronization procedure is described by Nobre *et al.* (2020) and Cardoso *et al.* (2008) and is schematically represented elsewhere [60, 61].

The micronized $CaAc_2$ was then collected and put through the same calcination process as the eggshells

to transform into calcium oxide to be used as a nanocatalyst in the transesterification of triglycerides present in the tested soybean oil to obtain FAME, i.e., biodiesel.

2.4. Catalyst characterization

2.4.1. Fourier Transform InfraRed (FTIR) spectroscopy

The ATR-FTIR equipment used was an Interspectrum spectrometer, model Interspec 200-X, with a maximum and minimum wavenumber of 4000 and 400 cm^{-1}, respectively, and with a spectrum resolution of 4 cm^{-1}.

2.4.2. Textural Characterization: N_2 adsorption/ desorption isotherms, Brunauer-Emmett-Teller (B.E.T.) surface area and micropore and mesopore volume

Textural characterisation was performed for the CaO, which was obtained directly from the calcination of the eggshells, and the calcium oxide, which was obtained from the micronization process using SAS. The surface areas were assessed by application of the Brunauer–Emmett–Teller (B.E.T.) method using liquid nitrogen adsorption/ desorption isotherms at -196 ºC (77 K).

The total pore volume was then calculated using the adsorbed volume of nitrogen at a relative pressure (p/p_0) of 0.95. The micropore volume (calculated as the intercept on the ordinate axis) and the external surface area (slope) was found by applying linear regression to the plot. The volume of mesopores was found by subtracting the total pore volume from the volume of micropores [62].

The isotherms were obtained using an Autosorb IQ apparatus from Quantachrome and degassed under vacuum at 90 ºC for 1 hour and then heated at 350 ºC for 5 h.

2.4.3. Scanning Electron Microscopy and Energy Dispersive X-Ray Spectroscopy (SEM-EDS)

Scanning Electron Microscopy (SEM) images were observed using an Electron microscope JEOL 7100F equipped with Oxford light elements EDS detector and EBDS detector and Thermo Scientific Phenom Pro X equipped with EDS detector to characterise the calcium oxide from eggshell calcination, the nanoscale calcium oxide and calcium acetate particle size.

2.4.4. Thermogravimetric analysis (TGA)

Thermogravimetric analysis was performed to investigate how the thermal decomposition of the studied calcium acetate samples into calcium oxide occurred during the calcination step. The used equipment was a TG-DSC Netzsch Setsys Evo 16. For each experiment, 5 mg of $CaAc_2$ was used and heated at 900 ºC at a rate of 10 ºC/min. For the TGA runs, blank runs were subtracted to remove buoyancy effects.

2.4.5. X-ray Diffraction (XRD)

The crystalline nature of the sorbents was investigated by X-ray diffraction (XRD). Diffractograms were recorded (at room temperature) using a Bruker AXS-D8 Advance powder diffractometer with a Bragg-Brentano geometry [(CuKa radiation source (λ = 0.15406 nm)], operating at 30 mA and 40 kV. The scanning range was set from 20 to 70° (2θ) and 5 to 70° (2θ), with a step size of 0.03° and a step time of 0.5 s. The DIFFRAC.EVA software (Bruker) and the crystallography open database (COD) were used to allow the identification of the crystalline phases.

2.5. Soybean oil transesterification

The transesterification reaction of the soybean oil was performed using either the CaO that resulted from the eggshell calcination or the micronized CaO. The transesterification reaction was performed in a 10 mL flask. Soybean oil was weighed (5 g) and heated in a water bath until the reaction temperature of 63 ºC was achieved. Inside the reaction flask, methanol and the catalyst were weighed, and the resulting mixture was placed in the same water bath as the oil. The mixture was stirred at high rpm and then heated until the reaction temperature was achieved. The reaction temperature was also the methanol boiling point, and hence the reaction was carried out using methanol reflux, and for that, a condenser was placed on top of the flask.

Tests were performed with different reaction times (one to five hours) and three different catalyst loadings (1 %wt, 3 %wt and 5 %wt) for preliminary purposes. A fixed methanol/oil molar ratio of 12:1 was used for these tests.

After the completion of the reaction, the catalyst was separated by vacuum filtration, and the two

remaining phases were placed in a separation funnel and left to settle overnight to ensure a complete separation between the two phases.

The yield of the transesterification reaction was then calculated by the following equation:

$$Biodiesel\ yield\ (\%) = \frac{Real\ weight\ of\ FAME}{Theoretical\ weight\ of\ FAME} \times 100 \quad (3)$$

The theoretical weight of FAME was then calculated based on the stoichiometry of the transesterification reaction.

3. Results and Discussion

3.1. Catalyst characterization

3.1.1. Fourier Transform InfraRed (FTIR) Spectroscopy for the Catalysts

An important feature of the SAS precipitation technique is its ability to obtain a high-purity product when compared to the starting material. Even though the $CaAc_2$ produced from the eggshells was not purified during the reaction, the recovered SAS product did not contain impurities. This is evident from ref. [60], which displays the FTIR analysis of the micronized calcium acetate compared to the commercially available and eggshell-produced versions.

When analyzing the obtained spectra for the three types of calcium acetate, one can conclude that the calcium acetate precipitated from SAS and the commercial calcium acetate appear very similar, as both FTIR spectra present transmittance bands at the same wavenumbers.

As for the calcium acetate obtained from eggshells, two bands appear uniquely for this species, meaning that some acetic acid residue might be left in the sample. The literature describes bands ~1700 cm^{-1} and ~1300 cm^{-1} to be specific to this acid [63].

The same analysis was also made for the CaO catalysts and compared with the starting material (eggshells), as shown in Figure 1.

When comparing the three species, one can again conclude that the SAS technique can alter the Particle Size Distribution as a purifying step. The band at 850 cm^{-1} (C-H bending vibration) that appears for both CaO from eggshells and the eggshells themselves is absent in the micronized CaO. This band is specific to calcium carbonate and is related to out-of-plane deformation of the CO_3^- anion [64, 65].

3.1.2. Brunauer-Emmett-Teller (B.E.T.) surface area, micropore and mesopore volume, and N_2 adsorption/desorption isotherms

Another aspect that was also studied for both catalysts was their textural properties. These properties can be correlated with the Particle Size Distribution that was considered before, which confirmed the success of the CaO micronization

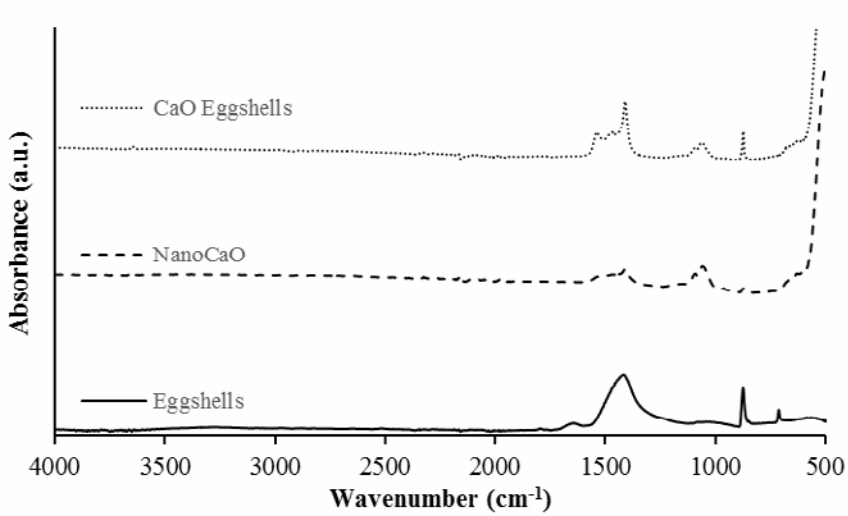

Figure 1. FTIR spectrum of the prepared catalysts (CaO from eggshells and nano CaO) and the eggshells used as feedstock.

by SAS precipitation. It is important to note that the primary objective of this work was to decrease the particle size of CaO so as to enhance the surface area of the catalyst and, consequently, its catalytic activity.

Firstly, the adsorption/desorption isotherms for nitrogen (N_2) at 77 K were traced for both solids, as shown in Figure 2 for CaO originating from the eggshells and Figure 3 for the micronized calcium oxide (Nano-CaO).

Considering the adsorption/desorption isotherms for CaO from the eggshells, displayed in Figure 2, and comparing with the literature, it is possible to conclude that the isotherm corresponds to an

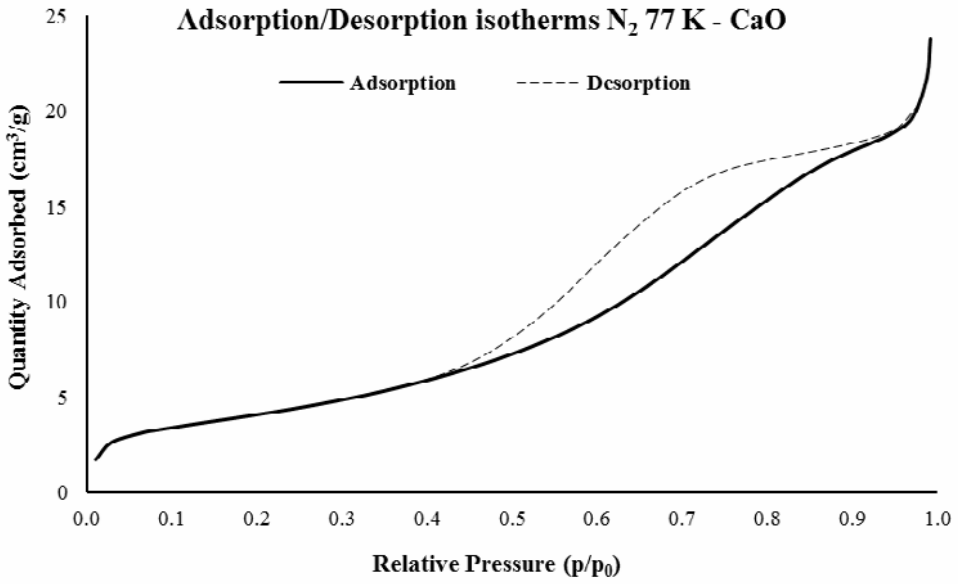

Figure 2. N_2 adsorption/desorption isotherms at 77 K for CaO from eggshells.

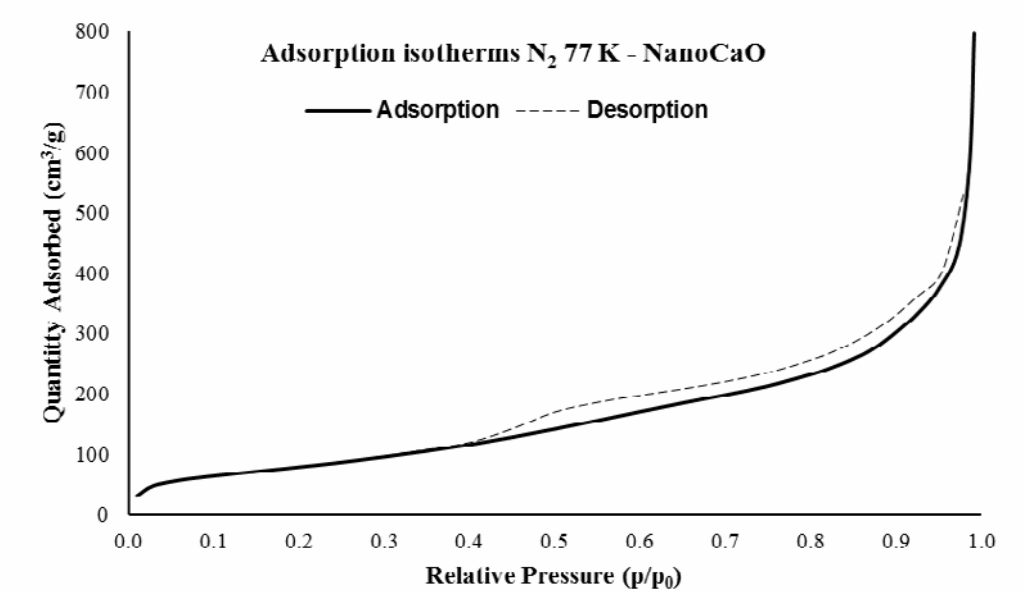

Figure 3. N_2 adsorption/desorption isotherms at 77 K for NanoCaO.

isotherm type IV, more specifically, an isotherm of type IV(a), which according to International Union of Pure and Applied Chemistry (IUPAC), are characteristic of mesoporous adsorbents. In these types of isotherms, the capillary condensation is always accompanied by hysteresis. Regarding the CaO from eggshells, the observed hysteresis is of type H1, meaning that this material exhibits quite a narrow range of uniform mesopores [66, 67].

Regarding the adsorption/desorption isotherms for NanoCaO and comparing with the literature and with Figure 2, it is possible to conclude that the isotherm is also of type IV(a), and the observed hysteresis in this case is of type H4, corresponding to an adsorption branch similar to a composition of isotherms of type I and type II and the noticeable uptake at low relative pressure is associated with the filling of the micropores. Another typical trait of this type of hysteresis is the sharp step-down of the desorption branch at relative pressure values around 0.4 – 0.5 [66].

Afterwards, the specific surface area (S_{BET}), the external surface area, and micro- and mesopore volumes were calculated. Table 1 displays the obtained results for the textural characterization of both types of calcium oxide.

When analyzing the contents of the table above, one can conclude that the micronization of calcium oxide indeed produced a massive increase in specific surface area, progressing from 15.257 m^2/g to 315.710 m^2/g, which is an increase of over 2000%. This also represents an increase in terms of external surface area, of a similar magnitude.

Considering the pore volume, the analysis of the adsorption/desorption isotherms for the two types of solids (Figure 3 and Figure 4) shows that both are mesoporous, as it is shown in Table 1.

3.1.3. Scanning Electron Microscopy and Energy Dispersive X-Ray Spectroscopy (SEM-EDS)

3.1.3.1. Scanning Electron Microscopy

Scanning Electron Microscopy was executed to assess calcium oxide and acetate morphology.

The morphology of the CaO obtained from the calcination of chicken eggshells showed well-formed and defined particles. The attained CaO structure showed several agglomerates of white granular solids with non-regular and unsymmetrical shapes.

The observed structure is very similar to the one described before. It was determined by comparing the obtained morphology with the ones observed in other studies. The only discernible difference between the different micrographs is the overall particle size; all of the micrographs showed white, non-regular solids.

By analyzing the SEM micrographs of the obtained CaO (Figure 2 of ref. [37], it was possible to assume a general particle size smaller than one micron (<1 μm), which is the most common dimension for CaO attained from the calcined eggshells. Even though the particles are smaller than 1 μm, they are not exactly nanoparticles. According to IUPAC, the dimensions of these particles must be within the 1-100 nm range.

As for the calcium oxide obtained from the calcination of the micronized calcium acetate, the SEM micrographs show (in Figure 4), just like in the SEM micrographs of the CaO attained from direct calcination of the eggshells, agglomerates of white granular solids having non-regular and unsymmetrical shape. However, the size of the micronized particles appears to be smaller.

As for the calcium acetate, its morphology shown in Figure 5, differs from other metallic acetates

Table 1. Textural characterization of both solids.

Sample	Specific Surface Area (S_{BET}) (m^2/g)	External Surface Area (m^2/g)	Total pore volume (cm^3/g)	Mesopore volume (cm^3/g)	Micropore Volume (cm^3/g)
CaO	15.26	6.99	18.93	18.92	0.018
NanoCaO	315.71	306.93	373.91	373.87	0.042

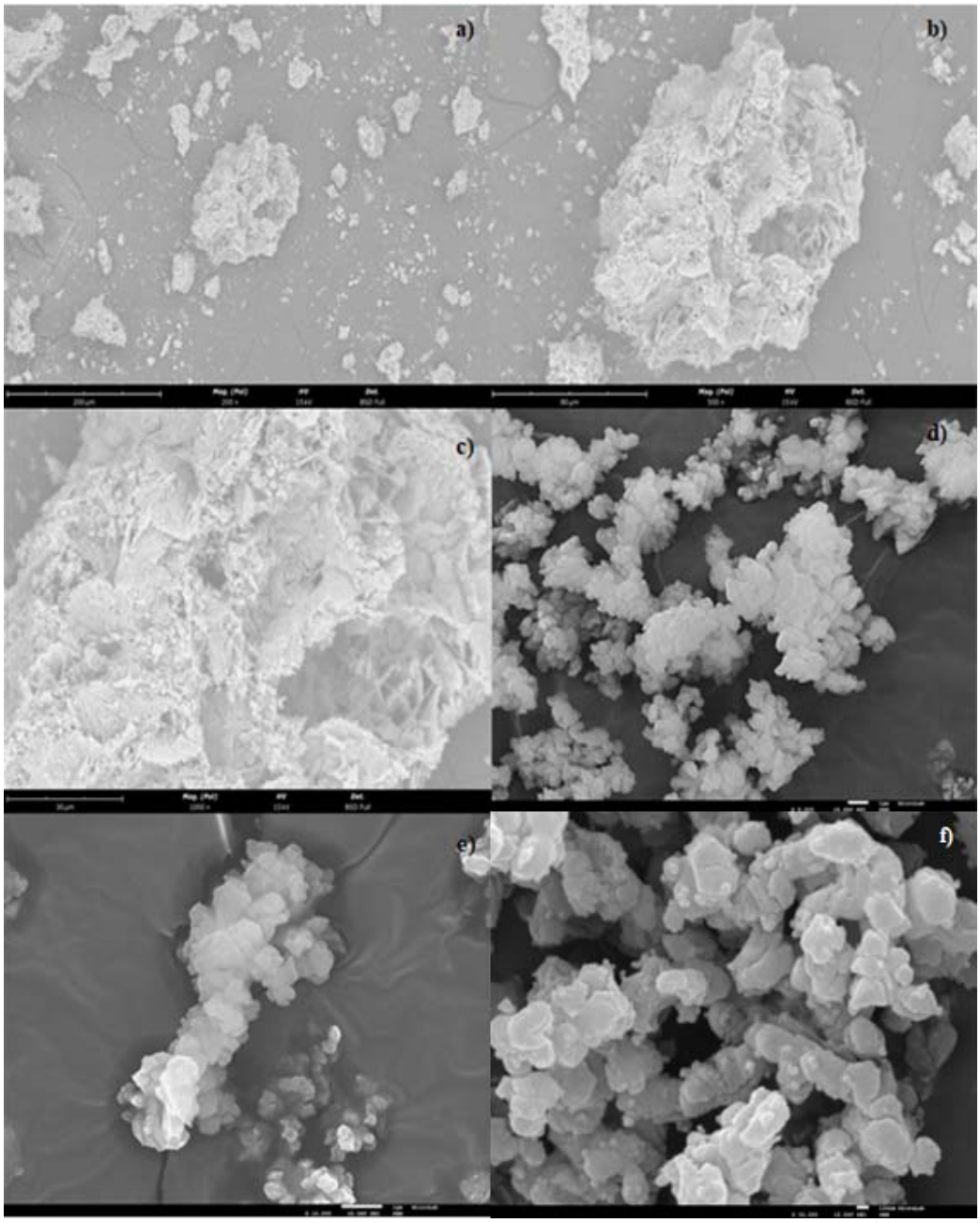

Figure 4. SEM images of nanoscale calcium oxide obtained from the calcination of the precipitated calcium acetate. Magnification and bars: a) 200x, 200 μm; b) 500x, 80 μm; c) 1000x, 30 μm; d) 5000x, 1 μm; e)10000x, 1 μm; f) 30000x, 100 nm.

obtained by SAS precipitation. Typically, particles obtained by SAS are spherical due to the explosion of "balloons" created by the expansion of the droplets formed in the nozzle.

The SEM micrographs for calcium acetate show particles bridged or linked between them, mostly associated with inefficient solvent removal, which was not the case in this work as solvent drying was performed for two hours to ensure the complete dryness of the product. As $CaAc_2$ is highly hygroscopic and is associated with the small particle size of the particle, increasing hydration

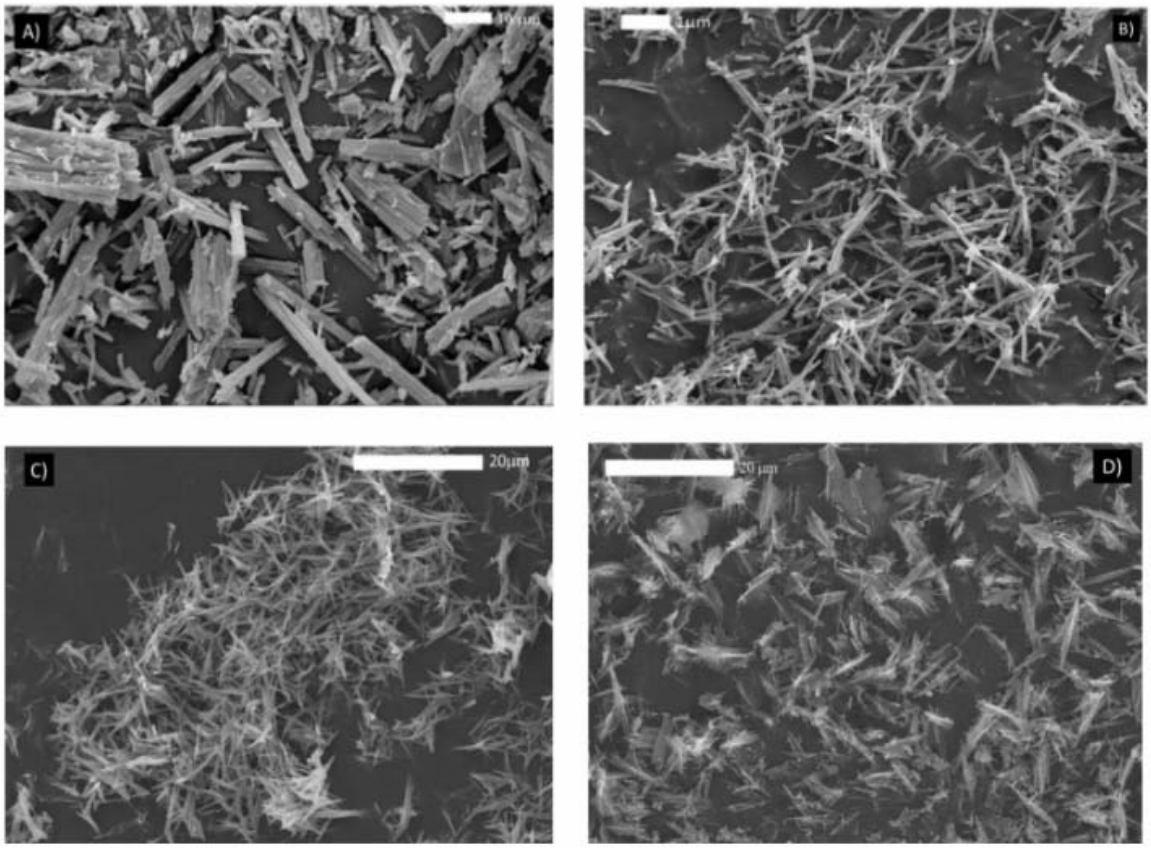

Figure 5. SEM images of calcium acetate: A) commercial calcium acetate without further treatment; B) precipitated calcium acetate at 50 ºC, 150 bar, 12.5 mg.mL^{-1} and 0.5 mL.min^{-1}; C) precipitated calcium acetate at 40 ºC, 200 bar, 20.0 mg.mL^{-1} and 0.5 mL.min^{-1}; D) precipitated calcium acetate at 60 ºC, 200 bar, 20.0 mg.mL^{-1} and 0.5 mL.min^{-1}.

of the compound can be an adequate explanation [60].

3.1.3.2. Energy Dispersive X-Ray Spectroscopy (EDS)

Energy Dispersive X-ray spectroscopy (EDS) was performed by using the same microscope and software employed for the SEM analysis. EDS provided a route to identify single atoms of chemical elements in the micronized calcium oxide sample [68].

Figure 6 depicts the EDS spectrum for the NanoCaO sample, and Table 2 displays the atomic composition of the sample.

By analyzing both Figure 6 and the data presented in Table 2, one can verify that the solid obtained from the calcination of the micronized $CaAc_2$ is CaO. Carbon atoms on the EDS spectrum are present as carbon tape is used to place the sample in the sample holder. This carbon tape is the background in the SEM micrograph of the selected sample region where the EDS scan was performed.

3.1.4. Particle size distribution

To confirm the success of the Supercritical Anti-Solvent (SAS) process, the particle size of CaO from eggshells and the NanoCaO was assessed. With the help of a measurement tool of an image processing software (in particular, the software Fiji), the assessment of particle size distribution was performed using the SEM micrographs presented before. The measurement tool was calibrated by considering the scale of the selected SEM micrographs.

Afterwards, lines were drawn on top of all the visible particles for each one of the solids. With

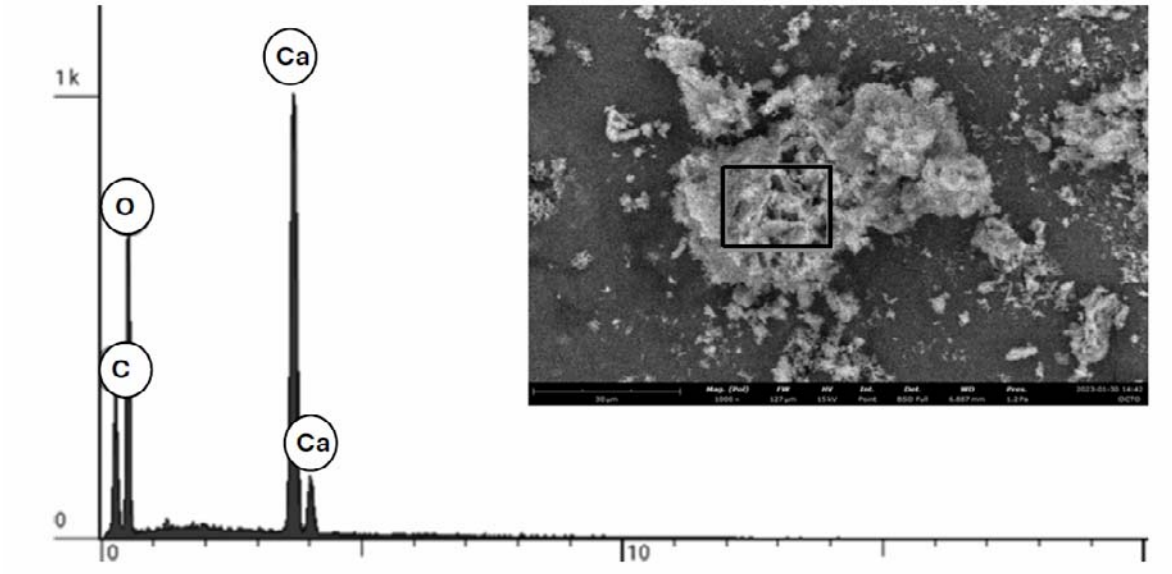

Figure 6. Left: Energy dispersive X-ray spectrum of micronized calcium oxide; Right: Sample portion chosen for single-atom identification.

Table 2. Elemental composition of the analyzed Nano-CaO.

Element Number	Element Symbol	Element Name	Atomic Concentration	Weight Concentration
6	C	Carbon	13.6	7.7
8	O	Oxygen	62.5	47.1
20	Ca	Calcium	24.9	45.1

the calibration previously performed, the measurement of the particles could be carried out, as shown in Figure 7.

Table 3 presents the statistical results from the Particle Size Distribution assessment for each solid.

With these results, the Gauss distribution curve was calculated and is shown in Figure 8.

Analyzing both Gaussian curves, it is possible to conclude that there are differences in the particle's distribution for both solids. In Figure 8, by comparing curves b) with a), it is possible to notice that there is a higher counting of particles below the 100 nm threshold (nanoscale region) in the NanoCaO sample (b) than in the CaO sample (a), meaning that there are more nanoparticles in NanoCaO than in CaO. The peak of the Gaussian curve (b) is also located below the 100 nm threshold, meaning that most of the particles present in the sample are in the nanoscale form, thus confirming the results shown in Table 3.

3.1.5. Thermogravimetric analysis

The thermogravimetric analysis was performed for three different types of $CaAc_2$ (calcium acetate).

Figure 6 of ref. [60] shows the thermogravimetry of $CaAc_2$. When studying the thermogravimetric graphic, it is possible to conclude that $CaAc_2$ prepared by SAS and the commercial one present similar profiles of thermal degradation that are comparable to the ones reported in the literature [69]. However, $CaAc_2$ produced directly from the eggshells (curve b, in Figure 6) loses about 10% of its mass at the end of the process, possibly due to the presence of water and other remaining impurities on the first stage of calcination. Between temperatures ranging from 400 °C to 500 °C, all the calcium acetate samples show a mass

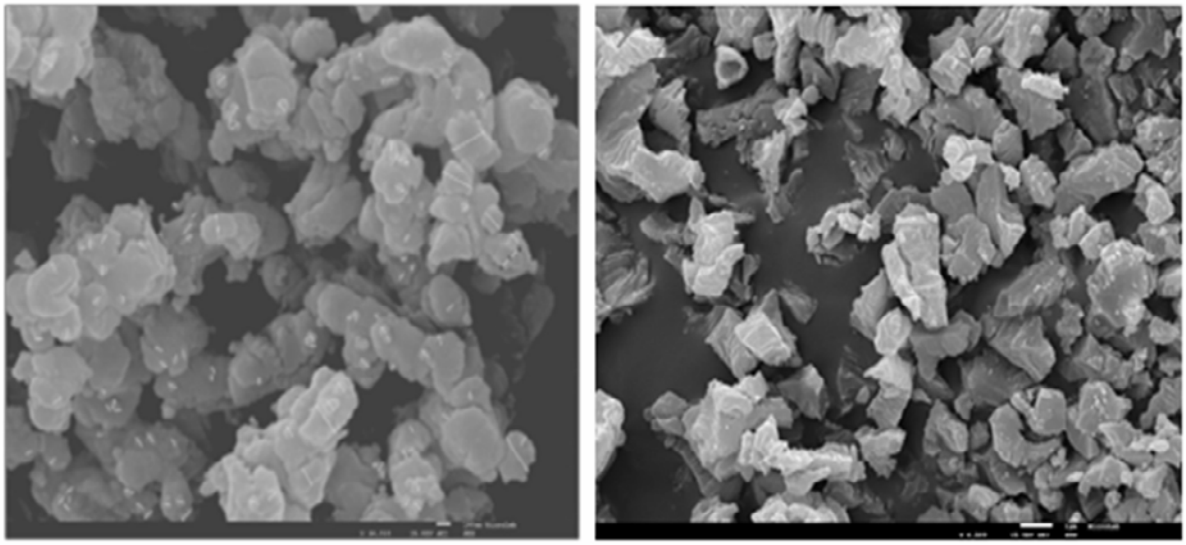

Figure 7. Measurement of the visible particles for both types of solids. Left: CaO from eggshells; Right: Nano-CaO.

Table 3. Statistical results from the particle size distribution assessment.

Catalyst	N total	Mean	Standard Deviation	Minimum	Median	Maximum
CaO	82.00	113.26	55.48	50.90	99.46	332.66
NanoCaO	147.00	77.44	70.48	23.07	56.33	453.73

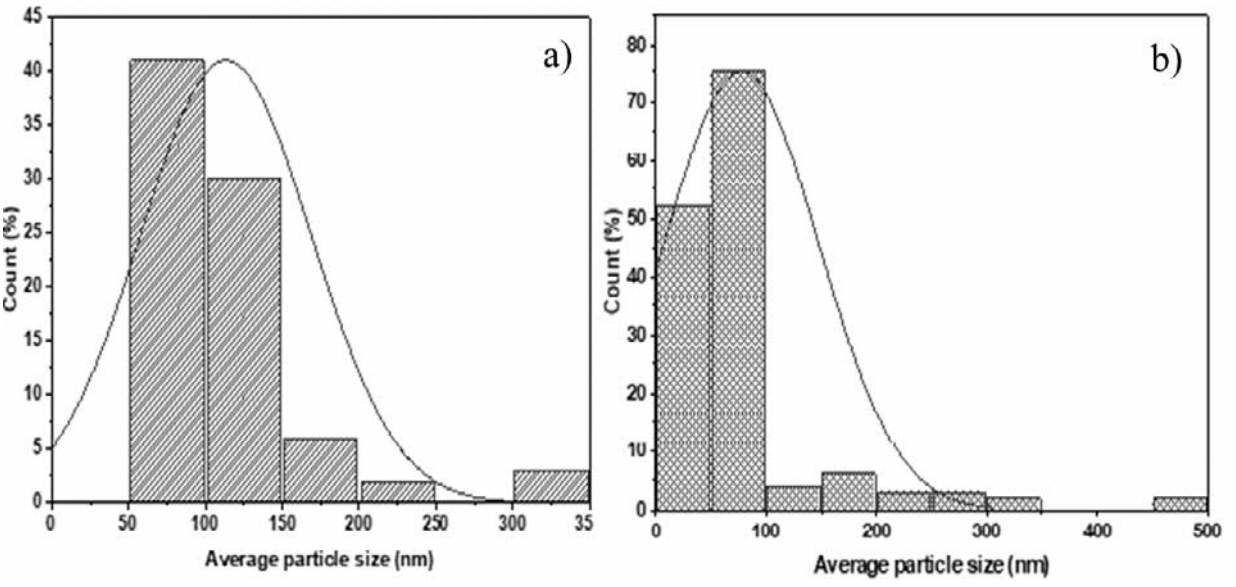

Figure 8. Gaussian distribution is based on the results obtained from the particle size distribution for both solids: a) CaO; b) NanoCaO.

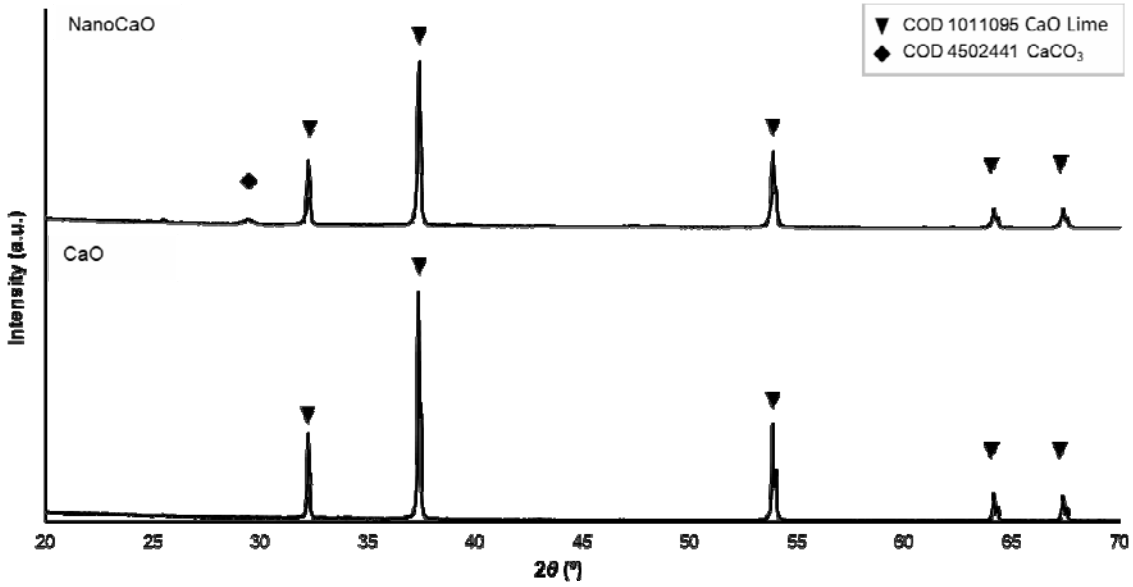

Figure 9. Diffractograms obtained for both types of CaO (calcium oxide).

loss between 40 to 50%, resulting from the release of acetone [$(CH3)_2CO$] during the conversion of calcium acetate into calcium carbonate ($CaCO_3$). Over the temperature of 700 °C, all the samples show an additional mass loss between 20-30%, corresponding to the release of carbon dioxide (CO_2) during the conversion of calcium carbonate into calcium oxide (CaO). A total mass loss of around 70% is expected during the transformation of calcium acetate into calcium oxide.

3.1.6. X-ray Diffraction (XRD)

To assess if micronization influences the crystallinity of the calcium oxide, both catalysts were characterized by X-ray diffraction.

Figure 9 shows the diffractograms for micronized calcium oxide (NanoCaO) and calcium oxide obtained from the calcination of eggshells (CaO) samples. Through the analysis of Figure 9, one can see that for the CaO sample, the only phase present is the one associated with lime (calcium oxide), as confirmed by the Crystallography Open Database (COD 1011095). With regard to the NanoCaO sample, the diffractogram is very similar to the one of CaO, with most of the peaks associated with lime. However, a peak is visible that the database identified as calcium carbonate ($CaCO_3$) (COD 4502441). It could also mean one of two things: incomplete calcination, or it began hydrating and carbonating. The first hypothesis is not possible since the calcination of the precursor was performed at 850 °C for three hours, which should be more than enough to guarantee the total conversion of carbonate into calcium oxide.

The second hypothesis appears to be more accurate. The literature mentions that natural calcium oxide is strongly hygroscopic and an excellent CO_2 absorber. Even though utmost care was taken when handling the sample after the calcination of the precursor (calcium acetate) to guarantee the non-hydration of NanoCaO, the fact is that it eventually happened. Having a higher surface area than the CaO derived from the calcination of the eggshells is a unique characteristic that makes NanoCaO a better catalyst, it is also a curse when it comes to hygroscopy. The higher volume of mesopores is perfect for heterogeneous catalysts, as it allows the reactants to diffuse inside their pores more easily. It also means that it has increased the hygroscopy of CaO. When in contact with water, CaO changes immediately into calcium hydroxide ($Ca(OH)_2$, which consequently reacts with the atmospheric CO_2, thus producing calcium carbonate [70–73].

3.2. Reaction of transesterification of soybean oil

As stated before, the transesterification reaction of soybean oil was performed using three different

catalyst loadings (1 %wt, 3 %wt and 5 %wt) using a methanol/oil molar ratio of 12:1. Figure 10 shows, for the same molar ratio of methanol/oil (12:1), that a loading of 5 %wt results in the best conversion of fatty acid, achieving a maximum of 85.83% conversion for three hours of reaction.

Although the obtained yields of the other two catalyst loadings are lower than for the 5 %wt loading, the results for the catalyst loading of 3 %wt show conversion yields close to those. A yield of 84.53% was obtained for this loading when the reaction lasted for two hours.

As for the lowest catalyst loading (1 %wt), the highest yield achieved was 77.27%.

The low yield values might be due to internal mass transfer limitations from the triglyceride particle to enter the CaO microporous, which results in a lower catalytic activity of the CaO particles. If the size of the CaO particles is reduced into nanoscale, their surface area would be higher, weakening the effect of internal mass transfer limitations, resulting in higher catalytic activity, higher transesterification yields, and shorter reaction times.

After Nobre *et al*. [60] performed the efficiency evaluation of the SAS process by implementing experimental design tools, namely Response Surface Methodology, this evaluation culminated in two operating conditions for the SAS process that presented better precipitation efficiencies, both at the same temperature (200 °C) and at different pressures (40 bar and 60 bar).

The calcium acetate obtained from micronization at those two operating conditions was then calcined to convert it into calcium oxide. Afterwards, this calcium oxide was used as a catalyst in trans-esterifying soybean oil into biodiesel. Figure 10 shows the yield percentage achieved for both catalysts and how it matched with the ones reached with the CaO obtained from eggshells.

It is possible to compare the results of transesterification reaction using the CaO from the eggshells and the CaO that went through the entire SAS process preparation. The catalyst loading used for both micronized catalysts was 1%wt. due to the small amount of precursor that could be produced. Nonetheless, both micronized CaO were evaluated.

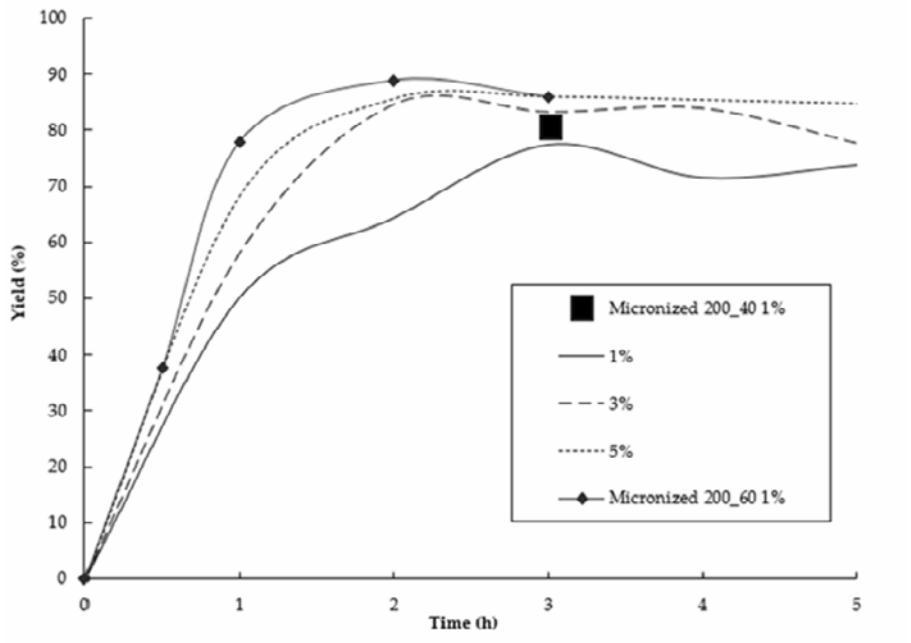

Figure 10. Effect of the reaction time on transesterification conversion yield for three different catalyst loadings and also the effect of micronisation on transesterification conversion.

Considering the CaO micronized at 200 °C and 40 bar, at the 3 hours reaction time mark, there is a slight enhancement in the reaction yield when compared with the CaO from eggshells at 1 %wt. of catalyst loading, resulting on an increase from 77% to 80%.

On the other hand, the CaO micronized at 200° C and 60 bar, at the same reaction time mark as the other micronized catalyst (3 hours), achieved a yield of around 85%, which translates into an increase of about 8% when compared with the same catalyst loading for CaO from eggshells. This is similar to the transesterification yield achieved with the CaO from eggshells at a catalyst loading of 5 %wt. Accordingly, at one fifth of the necessary amount, the catalyst micronized at 200 °C and 60 bar is just as capable as the CaO from eggshells at the maximum catalyst loading. Then, to assess how fast the reaction would be with this latter catalyst, the transesterification of soybean oil was performed at three different reaction times: thirty minutes, one hour and two hours. As can be seen in Figure 10, at the end of an hour of reaction time, the yield was as high as three hours of reaction for the same catalyst loading of CaO from eggshells, achieving a maximum yield of around 89% at the end of the second hour of reaction. As explained before, this could serve as proof of concept for the theory of decreasing the particle size to eliminate the diffusional constraints.

4. Conclusions

The scope of this study was to assess the influence of reducing the particle size of calcium oxide (CaO) on the efficiency of catalysis of the transesterification reaction of soybean oil to produce biodiesel. This reduction transformed the CaO from waste eggshells into nanocatalysts.

In summary, the micronization resulted in an enhancement of the specific surface area of the calcium oxide. Although the micronization was performed using calcium acetate as a precursor, chemical analysis of the obtained calcium oxide shows no contamination of other species. As a catalyst, the micronized calcium oxide showed great activity, showing results similar to the CaO from eggshells, at one fifth of the needed amount. Thus, it can be said that the micronization was successful.

FUNDING

This research was funded by FCT (Fundação para a Ciência e Tecnologia), grant number PD/BD/128450/2017; and by the European Union, under project UNPRECEDENTED: HORIZON-MSCA-2021-SE-01, Project 101086363.

CONFLICT OF INTEREST STATEMENT

The authors declare no conflicts of interest.

REFERENCES

1. Li, Y., Qiu, F., Yang, D., Li, X. And Sun, P. 2011, Biomass and Bioenergy, 35, 2787–2795.
2. Safaei-Ghomi, J., Ghasemzadeh, M. A. and Mehrabi, M. 2013, Scientia Iranica, 20, 549–554.
3. Shi, M., Zhang, P., Fan, M., Jiang, P. and Dong, Y. 2017, Fuel, 197, 343–347.
4. Ambat, I., Srivastava, V. and Sillanpää, M. 2018, Renewable and Sustainable Energy Reviews, 90, 356–369.
5. Parliament, T. H. E. E.; Union, P. European Parliament Directive 2009/30/EC. Official Journal of the European Union 2009, L140/88-L140/113.
6. Schöpe, M. 2008, Renewable Energy Directive. European Wind Energy Conference and Exhibition 2008, 1, 32–38.
7. Islam, A., Taufiq-Yap, Y. H., Chan, E.-S. S., Moniruzzaman, M., Islam, S. and Nabi, M. N. 2014, Energy Conversion and Management, 88, 1200–1218.
8. Meher, L. C., Vidya Sagar, D. and Naik, S. N. 2006, Renewable and Sustainable Energy Reviews, 10, 248–268.
9. Demirbas, A. 2009, Energy Conversion and Management 50, 14–34.
10. Mardhiah, H. H., Ong, H. C., Masjuki, H. H. H., Lim, S. and Lee, H. V. 2017, Renewable and Sustainable Energy Reviews, 67, 1225–1236.
11. Demirbas, A. 2007, Energy Policy, 35, 4661–4670.
12. Vyas, A. P., Verma, J. L. and Subrahmanyam, N. 2010, A Review on FAME Production Processes; Elsevier, 89, 1–9.
13. Dai, Y. M., Hsieh, C. H., Lin, J. H., Chen, F. H. and Chen, C. C. 2019, Catalysis, 9, 1–9.

14. Kouzu, M., Fujimori, A., Suzuki, T., Koshi, K. and Moriyasu, H. 2017, Fuel Processing Technology, 165, 94–101.
15. Narasimharao, K., Adam, L. and Karen, W. 2007, Journal of Biobased Materials and Bioenergy, 1, 19-30.
16. Zhang, X. L., Yan, S., Tyagi, R. D. and Surampalli, R. Y. 2013, Renewable and Sustainable Energy Reviews, 26, 216–223.
17. Vicente, G., Martínez, M. and Aracil, J. 2004, Bioresource Technology, 92, 297–305.
18. Leung, D. Y. C., Wu, X. and Leung, M. K. H. 2010, Applied Energy, 87, 1083–1095.
19. Fu, J., Chen, L., Lv, P., Yang, L. and Yuan, Z. 2015, Fuel, 154, 1–8.
20. Di Serio, M., Cozzolino, M., Giordano, M., Tesser, R., Patrono, P. and Santacesaria, E. 2007, Industrial & Engineering Chemistry Research, 46, 6379–6384.
21. Fonseca, J. M., Teleken, J. G., de Cinque Almeida, V. and da Silva, C. 2019, Energy Conversion and Management, 184, 205–218.
22. Brito, J. F. de, Ferreira, L. de O., Silva, J. P. da. and Ramalho, T. C. 2012, Química Nova, 35, 728–732.
23. Encinar, J. M. and Nogales-Delgado, S. 2020, Catalysis, 10, 1433.
24. Seminario-Calle, D., Ortega-Maldonado, M., Pinos-Vélez, V., Cisneros, J., Montero-Izquierdo, A., Echeverría-Paredes, P., Duque-Sarango, P. and Álvarez-Lloret, P. 2023, Urban Science, 7, 80.
25. Satapathy, A., Saikia, K. and Rokhum, S. 2023, Sustainability, 15, 11332.
26. Kesic, Z., Lukic, I., Zdujic, M., Mojovic, L. and Skala, D. 2016, Chemical Industry and Chemical Engineering Quarterly, 22, 391–408.
27. Gardy, J., Rehan, M., Hassanpour, A., Lai, X. and Nizami, A.-S. S. 2019, Journal of Environmental Management, 249.
28. Shu, Q., Gao, J., Nawaz, Z., Liao, Y., Wang, D. and Wang, J. 2010, Applied Energy, 87, 2589–2596.
29. Hattori, H. 2001, Applied Catalysis A: General, 222, 247–259.
30. Avhad, M. R. and Marchetti, J. M. 2016, Catalysis Reviews - Science and Engineering, 58, 157–208.
31. Refaat, A. A. 2011, International Journal of Environmental Science and Technology, 8, 203–221.
32. Shuit, S. H., Yee, K. F., Lee, K. T., Subhash, B. and Tan, S. H. 2013, RSC Advances, 3, 9070.
33. Yan, S., Kim, M., Salley, S. O. and Ng, K. Y. S. 2009, Applied Catalysis A: General, 360, 163–170.
34. Kiss, A. A., Dimian, A. C. and Rothenberg, G. 2006, Advanced Synthesis and Catalysis, 348, 75–81.
35. Chouhan, A. P. P. S. S. and Sarma, A. K. K. 2011, Renewable and Sustainable Energy Reviews, 15, 4378–4399.
36. Helwani, Z., Othman, M. R., Aziz, N., Kim, J. and Fernando, W. J. N. 2009, Applied Catalysis A: General, 363, 1–10.
37. Santos, S., Nobre, L., Gomes, J., Puna, J., Quinta-Ferreira, R. and Bordado, J. 2019, Energies, 12, 1–9.
38. Tsai, W. T., Yang, J. M., Lai, C. W., Cheng, Y. H., Lin, C. C. and Yeh, C. W. 2006, Bioresource Technology, 97, 488–493.
39. Hamester, M. R. R., Balzer, P. S. and Becker, D. 2012, Materials Research, 15, 204–208.
40. Mierzwa, D. 2009, Folia Malacologica, 16, 17–20.
41. Yoon, G. L., Kim, B. T., Kim, B. O. and Han, S. H. 2003, Waste Management, 23, 825–834.
42. Safi, B., Saidi, M., Daoui, A., Bellal, A., Mechekak, A. and Toumi, K. 2015, Construction and Building Materials, 78, 430–438.
43. Neves, N. M. and Mano, J. F. 2005, Materials Science and Engineering C, 25, 113–118.
44. Safi, B., Saidi, M., Daoui, A., Bellal, A., Mechekak, A. and Toumi, K. 2015, Construction and Building Materials, 78, 430–438.
45. Pinto, A. C., Guarieiro, L. L. N., Rezende, M. J. C., Ribeiro, N. M., Torres, E. A., Lopes, W. A.; Pereira, P. A. de P. and Andrade, J. B. de 2005, Journal of the Brazilian Chemical Society, 16, 1313–1330.
46. Islam, A. and Ravindra, P. 2016, Biodiesel Production with Green Technologies; Springer, ISBN 9783319452739.
47. Chaturvedi, S., Dave, P. N. and Shah, N. K. 2012, Journal of Saudi Chemical Society, 16, 307–325.

48. Rajput, N. 2015, International Journal of Advances in Engineering & Technology, 7, 1806–1811.
49. Santos, S., Puna, J., Gomes, J. and Marchetti, J. 2021, A Review on the Use of Bio/Nanostructured Heterogeneous Catalysts in Biodiesel Production. In Nano- and Biocatalysts for Biodiesel Production; Wiley, 59–91.
50. Su, W., Zhang, H., Xing, Y., Li, X., Wang, J. and Cai, C. 2021, Nanomaterials, 11, 1–14.
51. Tenorio, A., Gordillo, D. M., Pereyra, M. C. and Martínez de la Ossa, J. E. 2006, Industrial &amp Engineering Chemistry Research, 46, 114–123.
52. Reverchon, E. and Della Porta, G. 1999, Powder Technology, 106, 23–29.
53. Mahdi Pourmortazavi, S. and Somayyeh Hajimirsadeghi, S. 2005, Industrial &amp Engineering Chemistry Research, 44, 6523–6533.
54. Reverchon, E., Della Porta, G., Di Trolio, A. and Pace, S. 1998, Industrial &amp Engineering Chemistry Research, 37, 952–958.
55. Tang, Z. R., Edwards, J. K., Bartley, J. K., Taylor, S. H., Carley, A. F., Herzing, A. A., Kiely, C. J. and Hutchings, G. J. 2007, Journal of Catalysis, 249, 208–219.
56. Reverchon, E., Adami, R., Caputo, G. and De Marco, I. 2008, The Journal of Supercritical Fluids, 70–84.
57. Prosapio, V., De Marco, I., Scognamiglio, M. and Reverchon, E. 2015, Chemical Engineering Journal, 277, 286–294.
58. Reverchon, E., De Marco, I. and Torino, E. 2007, The Journal of Supercritical Fluids, 43, 126–138.
59. Fahim, T. K., Zaidul, I. S. M., Abu Bakar, M. R., Salim, U. M., Awang, M. B., Sahena, F., Jalal, K. C. A., Sharif, K. M. and Sohrab, M. H. 2014, Chemical Engineering and Processing: Process Intensification, 86, 47–52.
60. Nobre, L. C. S., Santos, S., Palavra, A. M. F., Calvete, M. J. F., de Castro, C. A. N. and Nobre, B. P. 2020, Journal of Supercritical Fluids, 163.
61. Cardoso, M. A. T., Monteiro, G. A., Cardoso, J. P., Prazeres, T. J. V., Figueiredo, J. M. F., Martinho, J. M. G., Cabral, J. M. S. and Palavra, A. M. F. 2008, The Journal of Supercritical Fluids, 44, 238–244.
62. Hudec, P., Smiešková, A., Idek, Z., Schneider, P. and Ŝolcová, O. 2002, Determination of Microporous Structure of Zeolites by T-Plot Method—State-of-the-Art. In Studies In Surface Science And Catalysis, 1587–1594.
63. Ryu, H.-S., Kim, D.-M., Shin, S.-H., Kim, W.-K., Lim, S.-M. and Park, W.-J. 2019, Sustainability, 11030879.
64. Tizo, M. S., Blanco, L. A. V., Cagas, A. C. Q., Dela Cruz, B. R. B., Encoy, J. C., Gunting, J. V., Arazo, R. O. and Mabayo, V. I. F. 2018, Sustainable Environment Research, 28, 326–332.
65. Busca, G. and Resini, C. 2006, Vibrational Spectroscopy for the Analysis of Geological and Inorganic Materials, ISBN 9780470027318.
66. Thommes, M., Kaneko, K., Neimark, A. V., Olivier, J. P., Rodriguez-Reinoso, F., Rouquerol, J. and Sing, K. S. W. 2015, Pure and Applied Chemistry, 87, 1051–1069.
67. Morishige, K. 2008, Adsorption, 14, 157–163.
68. Lovejoy, T. C., Ramasse, Q. M., Falke, M., Kaeppel, A., Terborg, R., Zan, R., Dellby, N. and Krivanek, O. L. 2012, Applied Physics Letters, 100, 2–6.
69. Musumeci, A. W., Frost, R. L. and Waclawik, E. R. 2007, Spectrochimica Acta - Part A: Molecular and Biomolecular Spectroscopy, 67, 649–661.
70. Bharti, P., Singh, B. and Dey, R. K. 2019, Journal of Nanostructure in Chemistry, 9, 269–280.
71. Ozkan, S., Puna, J. F., Gomes, J. F., Cabrita, T., Palmeira, J. V. and Santos, M. T. 2019, Energies, 12, 12224306.
72. Riza, M. A., Go, Y., Maier, R. R. J., Harun, S. W. and Anas, S. B. 2020, Sensors and Materials, 32, 3755–3772.
73. Morales-Flórez, V., Santos, A., Romero-Hermida, I. and Esquivias, L. 2015, Chemical Engineering Journal, 265, 194–200.